Eur. Phys. J. C 52, 805–811 (2007)
DOI 10.1140/epjc/s10052-007-0438-9

THE EUROPEAN PHYSICAL JOURNAL C

Regular Article – Experimental Physics

# Experimental studies of the $\pi^+\pi^-\pi^+\pi^-\pi^0$, $K^+K^-\pi^+\pi^-\pi^0$ and $p\bar{p}\pi^+\pi^-\pi^0$ final states produced in $e^+e^-$ annihilation at $\sqrt{s} = 3.773$ and $3.650\,\mathrm{GeV}$

The BES Collaboration

M. Ablikim[1], J.Z. Bai[1], Y. Ban[12], X. Cai[1], H.F. Chen[16], H.S. Chen[1], H.X. Chen[1], J.C. Chen[1], Jin Chen[1], Y.B. Chen[1], Y.P. Chu[1], Y.S. Dai[18], L.Y. Diao[9], Z.Y. Deng[1], Q.F. Dong[15], S.X. Du[1], J. Fang[1], S.S. Fang[1,19], C.D. Fu[15], C.S. Gao[1], Y.N. Gao[15], S.D. Gu[1], Y.T. Gu[4], Y.N. Guo[1], K.L. He[1], M. He[13], Y.K. Heng[1], J. Hou[11], H.M. Hu[1], J.H. Hu[3], T. Hu[1], X.T. Huang[13], X.B. Ji[1], X.S. Jiang[1], X.Y. Jiang[5], J.B. Jiao[13], D.P. Jin[1], S. Jin[1], Y.F. Lai[1], G. Li[1,20], H.B. Li[1], J. Li[1], R.Y. Li[1], S.M. Li[1], W.D. Li[1], W.G. Li[1], X.L. Li[1], X.N. Li[1], X.Q. Li[11], Y.F. Liang[14], H.B. Liao[1], B.J. Liu[1], C.X. Liu[1], F. Liu[6], Fang Liu[1], H.H. Liu[1], H.M. Liu[1], J. Liu[12,21], J.B. Liu[1], J.P. Liu[17], Jian Liu[1], Q. Liu[1], R.G. Liu[1], Z.A. Liu[1], Y.C. Lou[5], F. Lu[1], G.R. Lu[5], J.G. Lu[1], C.L. Luo[10], F.C. Ma[9], H.L. Ma[2], L.L. Ma[1,22], Q.M. Ma[1], Z.P. Mao[1], X.H. Mo[1], J. Nie[1], R.G. Ping[1], N.D. Qi[1], H. Qin[1], J.F. Qiu[1], Z.Y. Ren[1], G. Rong[1], X.D. Ruan[4], L.Y. Shan[1], L. Shang[1], D.L. Shen[1], X.Y. Shen[1], H.Y. Sheng[1], H.S. Sun[1], S.S. Sun[1], Y.Z. Sun[1], Z.J. Sun[1], X. Tang[1], G.L. Tong[1], D.Y. Wang[1,23], L. Wang[1], L.L. Wang[1], L.S. Wang[1], M. Wang[1], P. Wang[1], P.L. Wang[1], Y.F. Wang[1], Z. Wang[1], Z.Y. Wang[1], Zheng Wang[1], C.L. Wei[1], D.H. Wei[1], Y. Weng[1], N. Wu[1], X.M. Xia[1], X.X. Xie[1], G.F. Xu[1], X.P. Xu[6], Y. Xu[11], M.L. Yan[16], H.X. Yang[1], Y.X. Yang[3], M.H. Ye[2], Y.X. Ye[16], G.W. Yu[1], C.Z. Yuan[1], Y. Yuan[1], S.L. Zang[1], Y. Zeng[7], B.X. Zhang[1], B.Y. Zhang[1], C.C. Zhang[1], D.H. Zhang[1], H.Q. Zhang[1], H.Y. Zhang[1], J.W. Zhang[1], J.Y. Zhang[1], S.H. Zhang[1], X.Y. Zhang[13], Yiyun Zhang[14], Z.X. Zhang[12], Z.P. Zhang[16], D.X. Zhao[1], J.W. Zhao[1], M.G. Zhao[1,a], P.P. Zhao[1], W.R. Zhao[1], Z.G. Zhao[1,24], H.Q. Zheng[12], J.P. Zheng[1], Z.P. Zheng[1], L. Zhou[1], K.J. Zhu[1], Q.M. Zhu[1], Y.C. Zhu[1], Y.S. Zhu[1], Z.A. Zhu[1], B.A. Zhuang[1], X.A. Zhuang[1], B.S. Zou[1]

[1] Institute of High Energy Physics, P.O.Box 918-1, Beijing 100049, P.R. China
[2] China Center for Advanced Science and Technology (CCAST), Beijing 100080, P.R. China
[3] Guangxi Normal University, Guilin 541004, P.R. China
[4] Guangxi University, Nanning 530004, P.R. China
[5] Henan Normal University, Xinxiang 453002, P.R. China
[6] Huazhong Normal University, Wuhan 430079, P.R. China
[7] Hunan University, Changsha 410082, P.R. China
[8] Jinan University, Jinan 250022, P.R. China
[9] Liaoning University, Shenyang 110036, P.R. China
[10] Nanjing Normal University, Nanjing 210097, P.R. China
[11] Nankai University, Tianjin 300071, P.R. China
[12] Peking University, Beijing 100871, P.R. China
[13] Shandong University, Jinan 250100, P.R. China
[14] Sichuan University, Chengdu 610064, P.R. China
[15] Tsinghua University, Beijing 100084, P.R. China
[16] University of Science and Technology of China, Hefei 230026, P.R. China
[17] Wuhan University, Wuhan 430072, P.R. China
[18] Zhejiang University, Hangzhou 310028, P.R. China
[19] DESY, 22607, Hamburg, Germany
[20] Universite Paris XI, LAL-Bat. 208-BP34, 91898-ORSAY Cedex, France
[21] Max-Plank-Institut fuer Physik, Foehringer Ring 6, 80805 Munich, Germany
[22] University of Toronto, Toronto M5S 1A7, Canada
[23] CERN, 1211 Geneva 23, Switzerland
[24] University of Michigan, Ann Arbor, MI 48109, USA

Received: 12 September 2007 / Revised version: 22 September 2007 /
Published online: 17 October 2007 – 

**Abstract.** We report measurements of the observed cross sections for $e^+e^- \to \omega\pi^+\pi^-$, $\omega K^+K^-$, $\omega p\bar{p}$, $K^+K^-\rho^0\pi^0$, $K^+K^-\rho^+\pi^- + \text{c.c.}$, $K^{*0}K^-\pi^+\pi^0 + \text{c.c.}$, $K^{*+}K^-\pi^+\pi^- + \text{c.c.}$, $\phi\pi^+\pi^-\pi^0$ and $\Lambda\bar{\Lambda}\pi^0$ at $\sqrt{s} =$ 3.773 and 3.650 GeV. Upper limits (90% C.L.) are given for observed cross sections and for $\psi(3770)$ decay branching fractions for production of these final states. These measurements are made by analyzing the data sets of 17.3 $\text{pb}^{-1}$ collected at $\sqrt{s} = 3.773$ GeV and 6.5 $\text{pb}^{-1}$ collected at $\sqrt{s} = 3.650$ GeV with the BES-II detector at the BEPC collider.

## 1 Introduction

During the past thirty years, the $\psi(3770)$ resonance was expected to decay almost entirely into pure $D\bar{D}$ [1]. However, previous data suggest that the $\psi(3770)$ is not saturated by $D\bar{D}$ decays [2]. Recently, the BES Collaboration measured the branching fraction for $\psi(3770) \to$ non-$D\bar{D}$ decay to be about $(15 \pm 5)\%$ [3–5] with two different data samples and analysis methods. This indicates that the $\psi(3770)$ may substantially decay into charmless final states. In the last two years, many efforts have been undertaken by the BES [6–11] and CLEO [12–17] collaborations to search for charmless decays of $\psi(3770)$ but only upper limits were derived for most decay modes. So far, the results can not explain the discrepancy between the observed cross sections for $D\bar{D}$ and $\psi(3770)$ production. To understand this discrepancy, a comparison of observed cross sections for exclusive light-hadron final states at the center-of-mass energies of 3.773 GeV and below 3.660 GeV excluding the contributions from $J/\psi$, $\psi(3686)$ and $D\bar{D}$ decays could be helpful. A measurement of exclusive cross sections at these two or at more energy points can also provide valuable information to understand the mechanism of the continuum light-hadron production.

In this paper, we report measurements of the observed cross sections for the exclusive light-hadron final states, of $\omega\pi^+\pi^-$, $\omega K^+K^-$, $\omega p\bar{p}$, $K^+K^-\rho^0\pi^0$, $K^+K^-\rho^+\pi^- + \text{c.c.}$, $K^{*0}K^-\pi^+\pi^0 + \text{c.c.}$, $K^{*+}K^-\pi^+\pi^- + \text{c.c.}$, $\phi\pi^+\pi^-\pi^0$ and $\Lambda\bar{\Lambda}\pi^0$, produced in $e^+e^-$ annihilation, and derive upper limits for $\psi(3770)$ decays into these final states. The data sets used in the analysis were collected at $\sqrt{s} = 3.773$ and 3.650 GeV with the BES-II detector at the BEPC collider, which correspond to the integrated luminosities of 17.3 $\text{pb}^{-1}$ and 6.5 $\text{pb}^{-1}$, respectively. For convenience, we call these two data sets the $\psi(3770)$ resonance data and the continuum data in the paper, respectively.

## 2 BES-II detector

The BES-II is a conventional cylindrical magnetic detector that is described in detail in [18, 19]. A 12-layer vertex chamber(VC) surrounding a beryllium beam pipe provides input to event trigger, as well as coordinate information. A forty-layer main drift chamber (MDC) located just outside the VC yields precise measurements of charged particle trajectories with a solid angle coverage of 85% of $4\pi$; it also provides ionization energy loss ($\text{d}E/\text{d}x$) measurements for particle identification. Momentum resolution of $1.7\%\sqrt{1+p^2}$ ($p$ in GeV/$c$) and $\text{d}E/\text{d}x$ resolution of 8.5% for Bhabha scattering electrons are obtained for the data taken at $\sqrt{s} = 3.773$ GeV. An array of 48 scintillation counters surrounding the MDC measures time of flight (TOF) of charged particles with a resolution of about 180 ps for electrons. Outside the TOF counters, a 12 radiation length, lead-gas, six-readout-layer barrel shower counter (BSC), operating in limited streamer mode, measures the energies of electrons and photons over 80% of the total solid angle with an energy resolution of $\sigma_{\text{E}}/E = 0.22/\sqrt{E}$ ($E$ in GeV) and spatial resolutions of $\sigma_\phi = 7.9$ mrad and $\sigma_Z = 2.3$ cm for electrons. A solenoidal magnet outside the BSC provides a 0.4 T magnetic field in the central tracking region of the detector. Three double-layer muon counters instrument the magnet flux return and serve to identify muons with momentum greater than 500 MeV/$c$, with a solid angle coverage of 68%.

## 3 Event Selection

In selection of the above processes, the possible intermediate resonances are searched by analyzing the final states $\pi^+\pi^-\pi^+\pi^-\gamma\gamma$, $K^+K^-\pi^+\pi^-\gamma\gamma$ and $p\bar{p}\pi^+\pi^-\gamma\gamma$. The $\pi^0$, $\omega$, $\rho^0$, $\rho^+$, $K^{*0}$, $K^{*+}$, $\phi$ and $\Lambda$ particles are reconstructed by the decays $\pi^0 \to \gamma\gamma$, $\omega \to \pi^+\pi^-\pi^0$, $\rho^0 \to \pi^+\pi^-$, $\rho^+ \to \pi^+\pi^0$, $K^{*0} \to K^+\pi^-$, $K^{*+} \to K^+\pi^0$, $\phi \to K^+K^-$ and $\Lambda \to p\pi^-$, respectively. Throughout this paper, charge conjugation is implied.

To select the candidate events, we require the number of charged tracks to be four with total charge zero. Each charged track should be well reconstructed in the MDC with good helix fits and satisfy $|\cos\theta| < 0.85$, where $\theta$ is the polar angle. All tracks, save those from $\Lambda$ decays, must originate from the interaction region by requiring that the closest approaches of a charged track are less than 2.0 cm in the $xy$-plane and 20.0 cm in the $z$ direction.

The TOF and $\text{d}E/\text{d}x$ measurements for each charged track are used to calculate the confidence levels $CL_\pi$, $CL_K$ or $CL_p$ for the pion, kaon or proton hypotheses. The pion candidate is required to have a confidence level $CL_\pi$ greater than 0.1%. In order to reduce the misidentification, the kaon candidate is required to have the confidence level $CL_K$ greater than $CL_\pi$. For proton identification, the ratio $\frac{CL_p}{CL_\pi+CL_K+CL_p}$ is required to be greater than 0.6.

The BSC measurements are used to select photons. The energy of each good photon deposited in the BSC should be greater than 0.05 GeV, and the electromagnetic shower should start in the first five readout layers. The angle between the cluster development direction and the photon emission direction is required to be within 37° [20–22]. In order to reduce the radiative photons from charge

[a] e-mail: zhaomg@mail.ihep.ac.cn

particles, the angle between the photon and the nearest charged track is greater than 22° [20–22].

In order to improve mass resolution and suppress combinatorial background, an energy-momentum conservation kinematic fit is imposed on the $\pi^+\pi^-\pi^+\pi^-\gamma\gamma$, $K^+K^-\pi^+\pi^-\gamma\gamma$ or $p\bar{p}\pi^+\pi^-\gamma\gamma$ combination. In addition, we constrain the invariant mass of the two photons to the $\pi^0$ nominal mass. The candidates with a kinematic fit probability greater than 1% are accepted. If more than one combination remains after the above selection criteria, the combination with the largest fit probability is retained.

For the $K^+K^-\pi^+\pi^-\pi^0$ final state, we exclude the events from $D\bar{D}$ decays by rejecting the events in which the $D^0$ and $\bar{D}^0$ mesons can be reconstructed in the decay modes of $D^0 \to K^-\pi^+$ and $\bar{D}^0 \to K^+\pi^-\pi^0$ [23].

## 4 Data analysis

We search for possible intermediate resonances by examining the invariant mass spectra of the $\pi^+\pi^-\pi^0$, $\pi^+\pi^-$, $\pi^\pm\pi^0$, $K^\pm\pi^\mp$, $K^\pm\pi^0$, $K^+K^-$ and $p\pi^-/\bar{p}\pi^+$ combinations from the selected $\pi^+\pi^-\pi^+\pi^-\pi^0$, $K^+K^-\pi^+\pi^-\pi^0$ and $p\bar{p}\pi^+\pi^-\pi^0$ events. The invariant masses of these combinations are calculated with the fitted momentum vectors from the kinematic fit. In the paper, they are denoted by $M_{\pi^+\pi^-\pi^0}$, $M_{\pi^+\pi^-}$, $M_{\pi^\pm\pi^0}$, $M_{K^\pm\pi^\mp}$, $M_{K^\pm\pi^0}$, $M_{K^+K^-}$ and $M_{p\pi^-/\bar{p}\pi^+}$, respectively.

### 4.1 Candidates for $e^+e^- \to \omega\pi^+\pi^-$, $e^+e^- \to \omega K^+K^-$ and $e^+e^- \to \omega p\bar{p}$

To investigate the processes $e^+e^- \to \omega\pi^+\pi^-$, $e^+e^- \to \omega K^+K^-$, and $e^+e^- \to \omega p\bar{p}$, we analyze the invariant masses of the $\pi^+\pi^-\pi^0$ combinations from the selected $\pi^+\pi^-\pi^+\pi^-\pi^0$, $K^+K^-\pi^+\pi^-\pi^0$ and $p\bar{p}\pi^+\pi^-\pi^0$ events. Figure 1 shows the invariant mass distributions from the selected final states. The mass window of $\pm 40\,\mathrm{MeV}/c^2$ (accounting for the $\omega$ width [24] and its mass resolution determined by Monte Carlo simulation) around the $\omega$ nominal mass is taken as the $\omega$ signal region. Counting the events with $M_{\pi^+\pi^-\pi^0}$ in the $\omega$ signal regions, we obtain the numbers of the events in the signal region for searching for the signal events $e^+e^- \to \omega\pi^+\pi^-$, $e^+e^- \to \omega K^+K^-$ and $e^+e^- \to \omega p\bar{p}$ observed from the $\psi(3770)$ resonance data (left) and the continuum data (right), respectively. The numbers of the events observed in the $\omega$ signal regions are listed in the second columns in Tables 1 and 2.

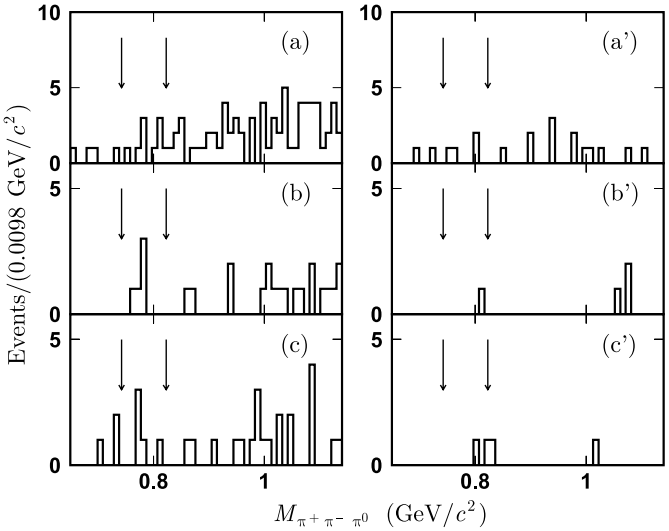


**Fig. 1.** The distributions of the invariant masses of the $\pi^+\pi^-\pi^0$ combinations from the selected **a** $\pi^+\pi^-\pi^+\pi^-\pi^0$, **b** $K^+K^-\pi^+\pi^-\pi^0$ and **c** $p\bar{p}\pi^+\pi^-\pi^0$ events from the $\psi(3770)$ resonance data (*left*) and the continuum data (*right*)

### 4.2 Further analyses of the $K^+K^-\pi^+\pi^-\pi^0$ final state

Figure 2 shows the invariant masses of the $K^\pm\pi^\mp$ and $K^\pm\pi^0$ combinations from the selected $K^+K^-\pi^+\pi^-\pi^0$ events. In each figure, the $K^*$ signal is clearly observed. Fitting to these invariant mass spectra with a Breit–Wigner convoluted with a Gaussian resolution function for the $K^*$ signal and a second polynomial for the background,

**Table 1.** The observed cross sections for $e^+e^- \to f$ at $\sqrt{s} = 3.773$ GeV, where $N^{\rm obs}$ is the number of events observed from the $\psi(3770)$ resonance data, $N^b$ is the number of total background events, $N^{\rm net}$ is the number of the signal events, $N^{\rm up}$ is the upper limit on the number of the signal events, $\epsilon$ is the detection efficiency, $\Delta_{\rm sys}$ is the relative systematic error in the measurement, $\sigma$ is the observed cross section and $\sigma^{\rm up}$ is the upper limit on the observed cross section at 90% C.L.

| $e^+e^- \to$ | $N^{\rm obs}$ | $N^b$ | $N^{\rm net}$ (or $N^{\rm up}$) | $\epsilon$[%] | $\Delta_{\rm sys}$ | $\sigma$ (or $\sigma^{\rm up}$) [pb] |
|---|---|---|---|---|---|---|
| $\omega\pi^+\pi^-$ | 9 | 0 | $< 15.30$ | $3.06 \pm 0.08$ | 0.116 | $< 37.1$ |
| $\omega K^+K^-$ | 5 | 0 | $< 9.99$ | $1.67 \pm 0.06$ | 0.118 | $< 44.5$ |
| $\omega p\bar{p}$ | 5 | 0 | $< 9.99$ | $3.69 \pm 0.09$ | 0.124 | $< 20.3$ |
| $K^+K^-\rho^0\pi^0$ | 0 | 0 | $< 2.44$ | $2.90 \pm 0.05$ | 0.114 | $< 5.6$ |
| $K^+K^-\rho^+\pi^- + \text{c.c.}$ | $48.6 \pm 15.4$ | $2.7 \pm 0.9$ | $45.9 \pm 15.4$ | $2.85 \pm 0.10$ | 0.124 | $94.2 \pm 31.6 \pm 11.7$ |
| $K^{*0}K^-\pi^+\pi^0 + \text{c.c.}$ | $41.2 \pm 11.2$ | $1.3 \pm 0.7$ | $39.9 \pm 11.2$ | $3.01 \pm 0.08$ | 0.172 | $116.3 \pm 32.7 \pm 20.0$ |
| $K^{*+}K^-\pi^+\pi^- + \text{c.c.}$ | $22.3 \pm 9.1$ | $0.7 \pm 0.2$ | $21.6 \pm 9.1$ | $2.18 \pm 0.07$ | 0.150 | $173.9 \pm 73.3 \pm 26.1$ |
| $\phi\pi^+\pi^-\pi^0$ | 2 | 0 | $< 5.91$ | $3.11 \pm 0.06$ | 0.115 | $< 25.5$ |
| $\Lambda\bar{\Lambda}\pi^0$ | 0 | 0 | $< 2.44$ | $5.02 \pm 0.07$ | 0.123 | $< 7.9$ |

**Table 2.** The observed cross sections for $e^+e^- \to f$ at $\sqrt{s} = 3.650$ GeV, where $N^{\rm obs}$ is the number of events observed from the continuum data. The definitions of the other symbols are the same as those in Table 1

| $e^+e^- \to$ | $N^{\rm obs}$ | $N^b$ | $N^{\rm net}$ (or $N^{\rm up}$) | $\epsilon$[%] | $\Delta_{\rm sys}$ | $\sigma$ (or $\sigma^{\rm up}$) [pb] |
|---|---|---|---|---|---|---|
| $\omega\pi^+\pi^-$ | 4 | 0 | $< 8.60$ | $3.34 \pm 0.09$ | 0.116 | $< 50.9$ |
| $\omega K^+K^-$ | 1 | 0 | $< 4.36$ | $1.62 \pm 0.06$ | 0.119 | $< 53.4$ |
| $\omega p\bar{p}$ | 2 | 0 | $< 5.91$ | $3.81 \pm 0.09$ | 0.124 | $< 30.9$ |
| $K^+K^-\rho^0\pi^0$ | $11.4 \pm 6.4$ | $2.3 \pm 0.9$ | $9.1 \pm 6.4$ | $2.98 \pm 0.05$ | 0.224 | $47.6 \pm 33.4 \pm 10.7$ |
| $K^+K^-\rho^+\pi^- + $c.c. | $27.0 \pm 10.0$ | $0.4 \pm 0.3$ | $26.6 \pm 10.0$ | $2.92 \pm 0.10$ | 0.139 | $141.9 \pm 53.3 \pm 19.7$ |
| $K^{*0}K^-\pi^+\pi^0 + $c.c. | $17.5 \pm 7.9$ | $0.5 \pm 0.4$ | $17.0 \pm 7.9$ | $3.10 \pm 0.08$ | 0.140 | $128.1 \pm 59.5 \pm 17.9$ |
| $K^{*+}K^-\pi^+\pi^- + $c.c. | $9.7 \pm 5.6$ | $0.6 \pm 0.6$ | $9.1 \pm 5.6$ | $2.25 \pm 0.07$ | 0.149 | $189.0 \pm 116.3 \pm 28.2$ |
| $\phi\pi^+\pi^-\pi^0$ | 2 | 0 | $< 5.91$ | $3.17 \pm 0.06$ | 0.115 | $< 66.7$ |
| $\Lambda\bar{\Lambda}\pi^0$ | 0 | 0 | $< 2.44$ | $4.95 \pm 0.07$ | 0.123 | $< 21.4$ |

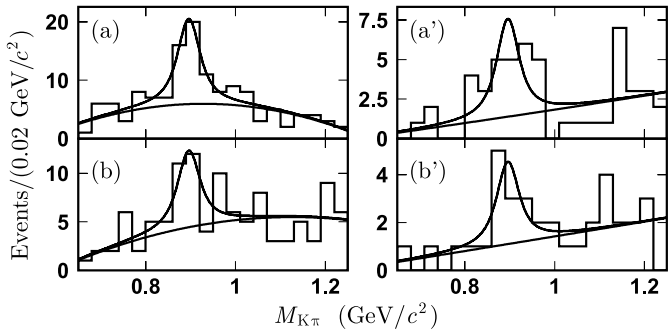


**Fig. 2.** The distributions of the invariant masses for the **a** $K^\pm\pi^\mp$ and **b** $K^\pm\pi^0$ combinations from the selected $K^+K^-\pi^+\pi^-\pi^0$ events from the $\psi(3770)$ resonance data (*left*) and the continuum data (*right*)

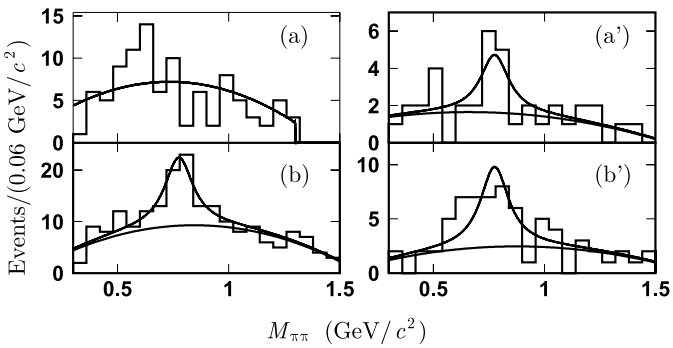


**Fig. 3.** The distributions of the invariant masses of the **a** $\pi^+\pi^-$ and **b** $\pi^\pm\pi^0$ combinations from the selected $K^+K^-\pi^+\pi^-\pi^0$ events from the $\psi(3770)$ resonance data (*left*) and the continuum data (*right*)

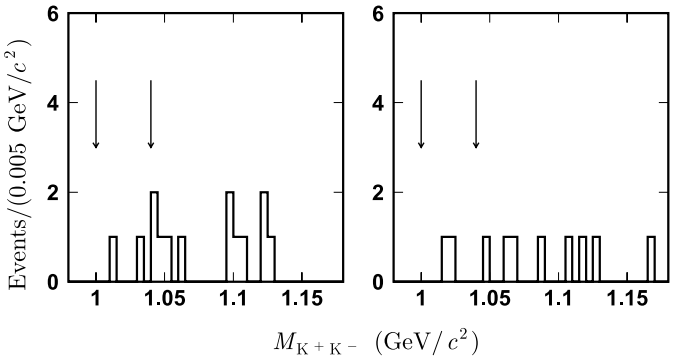


**Fig. 4.** The distributions of the invariant masses of the $K^+K^-$ combinations from the selected $K^+K^-\pi^+\pi^-\pi^0$ events from the $\psi(3770)$ resonance data (*left*) and the continuum data (*right*), where the pairs of arrows represent the $\phi$ signal regions

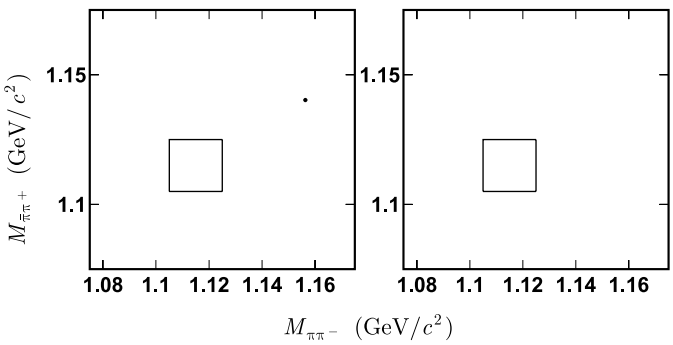


**Fig. 5.** The scatter plots of $M_{p\pi^-}$ versus $M_{\bar{p}\pi^+}$ from the selected $p\bar{p}\pi^+\pi^-\pi^0$ events from the $\psi(3770)$ resonance data (*left*) and the continuum data (*right*), where the rectangle regions show the $\Lambda$ and $\bar{\Lambda}$ signal regions

we obtain the numbers $N^{\rm obs}$ of the signal events for $e^+e^- \to K^{*0}K^-\pi^+\pi^0 + $c.c. and $e^+e^- \to K^{*+}K^-\pi^+\pi^- + $ c.c. observed from the $\psi(3770)$ resonance data (left) and the continuum data (right). These numbers are summarized in the second columns of Tables 1 and 2. In the fits, the mass and width of $K^*$ are fixed to the PDG values [24].

Figure 3 shows the invariant mass spectra of the $\pi^+\pi^-$ and $\pi^\pm\pi^0$ combinations from the selected $K^+K^-\pi^+\pi^-\pi^0$ events. Fitting to these invariant mass spectra with a Breit-Wigner convoluted with a Gaussian resolution function for the $\rho$ signal and a second order polynomial for the background, we obtain the numbers $N^{\rm obs}$ of the signal events for $e^+e^- \to K^+K^-\rho^0\pi^0$ and $e^+e^- \to K^+K^-\rho^+\pi^- + $c.c. from the $\psi(3770)$ data (left) and the continuum data (right), which are shown in the second columns of Tables 1 and 2. In the fits, the mass and width of $\rho$ are fixed to the PDG values [24].

Figure 4 shows the distributions of the invariant masses of the $K^+K^-$ combinations from the selected $K^+K^-\pi^+\pi^-\pi^0$ events. The mass window of $\pm 20\,\mathrm{MeV}/c^2$ around the $\phi$ nominal mass is taken as the $\phi$ signal region [10]. Selecting the events with $M_{K^+K^-}$ in the $\phi$ signal regions, we obtain 2 events in the signal region for searching for the $\phi\pi^+\pi^-\pi^0$ final state observed from both the $\psi(3770)$ resonance data (left) and the continuum data (right).

### 4.3 Further analyses of the $p\bar{p}\pi^+\pi^-\pi^0$ final state

The scatter plots of $M_{p\pi^-}$ versus $M_{\bar{p}\pi^+}$ from the selected $p\bar{p}\pi^+\pi^-\pi^0$ events are shown in Fig. 5. The mass window of $\pm 10\,\mathrm{MeV}/c^2$ around the $\Lambda$ nominal mass is taken as the $\Lambda$ signal region, determined by Monte Carlo simulation. In the $\Lambda\bar{\Lambda}\pi^0$ signal region in each figure, no signal event for the $\Lambda\bar{\Lambda}\pi^0$ final state is observed from the two data sets.

## 5 Background subtraction

For the selected candidate events, there are the contributions from $J/\psi$ and $\psi(3686)$ decays due to ISR (initial state radiation) process. In addition, there are the contaminations from the other final states due to misidentification between charged pions and kaons, or due to missing photon(s), etc.. Above the $D\bar{D}$ threshold, there are also the contributions from $D\bar{D}$ decays. The number $N^b$ of these contributions should be subtracted from the number $N^{\mathrm{obs}}$ of the selected events. These can be estimated by Monte Carlo simulation, which has been discribed in [10] in detail.

In the following analyses, we ignore the interference effects between the continuum and resonance amplitudes, since we don't know the details about the two amplitudes. In this case, subtracting $N^b$ from $N^{\mathrm{obs}}$, the numbers $N^{\mathrm{net}}$ of the signal events for the final states $e^+e^- \to K^+K^-\rho^0\pi^0$, $e^+e^- \to K^+K^-\rho^+\pi^- + \mathrm{c.c.}$, $e^+e^- \to K^{*0}K^-\pi^+\pi^0 + \mathrm{c.c.}$ and $e^+e^- \to K^{*+}K^-\pi^+\pi^- + \mathrm{c.c.}$ are obtained.

For the other final states, only a few events are observed from the data sets. We set the upper limits $N^{\mathrm{up}}$ on these numbers of the signal events by using the Feldman–Cousins method [25] in the absence of background at 90% confidence level (C.L.). These numbers are listed in Tables 1 and 2.

## 6 Results

### 6.1 Monte Carlo efficiency

The detection efficiencies for reconstruction of the events of $e^+e^- \to$ *exclusive light hadrons* are estimated by Monte Carlo simulation with a phase space generator for the BESII detector [26], including initial state radiation and photon vacuum polarization corrections [27] with $1/s$ cross section energy dependence. Final state radiation [28] decreases the detection efficiency by not more than 0.5%. Detailed Monte Carlo analysis gives the detection efficiency for each final state at $\sqrt{s} = 3.773$ and 3.650 GeV. They are summarized in Tables 1 and 2. For the final states containing $\pi^0$, $\omega$, $\rho^0$, $\rho^+$, $K^{*0}$, $K^{*+}$, $\phi$ and $\Lambda$ particles, the branching fractions for the decays $\pi^0 \to \gamma\gamma$, $\omega \to \pi^+\pi^-\pi^0$, $\rho^0 \to \pi^+\pi^-$, $\rho^+ \to \pi^+\pi^0$, $K^{*0} \to K^+\pi^-$, $K^{*+} \to K^+\pi^0$, $\phi \to K^+K^-$ and $\Lambda \to p\pi^-$ are set to be 100% in the generator. They are corrected with their branching fractions quoted from PDG [24], see (1) and (2).

### 6.2 Systematic error

The systematic errors in the measurement of the observed cross section for $e^+e^- \to$ *exclusive light hadrons* arise mainly from the uncertainties in luminosity ($\sim 2.1\%$ [3, 4]), photon selection ($\sim 2.0\%$ per photon), tracking efficiency ($\sim 2.0\%$ per track), charged particle identification ($\sim 0.5\%$ per pion or kaon, $\sim 2.0\%$ per proton), kinematic fit ($\sim 1.5\%$), Monte Carlo statistics [$\sim (1.2 \sim 3.9)\%$], branching fractions quoted from PDG [24] [$\sim 0.03\%$ for $\mathcal{B}(\pi^0 \to \gamma\gamma)$, $\sim 0.79\%$ for $\mathcal{B}(\omega \to \pi^+\pi^-\pi^0)$, $\sim 1.22\%$ for $\mathcal{B}(\phi \to K^+K^-)$ and $\sim 0.78\%$ for $\mathcal{B}(\Lambda \to p\pi^-)$], background subtraction [$\sim (0.0 \sim 13.4)\%$], fit to mass spectrum [$\sim (1.9 \sim 16.5)\%$], and Monte Carlo modeling ($\sim 6.0\%$ [10]). The total systematic errors $\Delta_{\mathrm{sys}}$ for each final state at $\sqrt{s} = 3.773$ and 3.650 GeV are obtained by adding these uncertainties in quadrature, respectively, which are shown in Tables 1 and 2.

### 6.3 Observed cross section or its upper limit for $e^+e^- \to f$

The observed cross section for $e^+e^- \to f$ is determined by

$$\sigma_{e^+e^-\to f} = \frac{N^{\mathrm{net}}}{\mathcal{L} \times \epsilon[\times \prod_i^n B_i]}\,, \qquad (1)$$

where $\mathcal{L}$ is the integrated luminosity of the data set, $N^{\mathrm{net}}$ is the number of the signal events for $e^+e^- \to f$, $\epsilon$ is the detection efficiency for the final state. Here, $n = 1$ or 2 or 3, is the number of the intermediate resonances in the final state, $B_i$ denotes the branching fraction [24] for the intermediate resonance decay, such as $\mathcal{B}(\pi^0 \to \gamma\gamma)$, $\mathcal{B}(\omega \to \pi^+\pi^-\pi^0)$, $\mathcal{B}(\phi \to K^+K^-)$ and $\mathcal{B}(\Lambda \to p\pi^-)$ etc. Inserting the corresponding numbers in (1), we obtain the observed cross sections for the final states $e^+e^- \to K^+K^-\rho^0\pi^0$, $e^+e^- \to K^+K^-\rho^+\pi^- + \mathrm{c.c.}$, $e^+e^- \to K^{*0}K^-\pi^+\pi^0 + \mathrm{c.c.}$ and $e^+e^- \to K^{*+}K^-\pi^+\pi^- + \mathrm{c.c.}$ at $\sqrt{s} = 3.773$ and 3.650 GeV, respectively. They are summarized in Tables 1 and 2, where the first error is statistical and the second systematic.

For the other final states for which only a few events are observed from the data, the upper limits on their observed cross section are set by

$$\sigma^{\mathrm{up}}_{e^+e^-\to f} = \frac{N^{\mathrm{up}}}{\mathcal{L} \times \epsilon \times (1 - \Delta_{\mathrm{sys}})[\times \prod_i^n B_i]}\,, \qquad (2)$$

**Table 3.** The upper limits on the observed cross section $\sigma^{\rm up}_{\psi(3770)\to f}$ and the branching fraction $\mathcal{B}^{\rm up}_{\psi(3770)\to f}$ for $\psi(3770)\to f$ are set at 90% C.L.. The $\sigma_{\psi(3770)\to f}$ in the second column is calculated with (3), where the first error is the statistical, the second is the mode-dependent systematic, and the third is the common systematic error. Here, the upper$^t$ denotes that we treat the upper limit on the observed cross section for $e^+e^-\to f$ at 3.773 GeV as $\sigma^{\rm up}_{\psi(3770)\to f}$, the upper$^n$ denotes that we neglect the contribution from the continuum production, and the upper$^z$ denotes that we treat the central value of $\sigma_{\psi(3770)\to f}$ as zero if it is less than zero

| Decay mode | $\sigma_{\psi(3770)\to f}$ [pb] | $\sigma^{\rm up}_{\psi(3770)\to f}$ [pb] | $\mathcal{B}^{\rm up}_{\psi(3770)\to f}$ [$\times 10^{-3}$] |
|---|---|---|---|
| $\omega\pi^+\pi^-$ | $< 37.1^{tn}$ | $< 37.1$ | $< 5.5$ |
| $\omega K^+K^-$ | $< 44.5^{tn}$ | $< 44.5$ | $< 6.6$ |
| $\omega p\bar{p}$ | $< 20.3^{tn}$ | $< 20.3$ | $< 3.0$ |
| $K^+K^-\rho^0\pi^0$ | $< 5.6^{tn}$ | $< 5.6$ | $< 0.8$ |
| $K^+K^-\rho^+\pi^-$ + c.c. | $-38.6\pm59.0\pm11.9\pm4.4^z$ | $< 99.0$ | $< 14.6$ |
| $K^{*0}K^-\pi^+\pi^0$ + c.c. | $-3.6\pm64.6\pm18.2\pm0.4^z$ | $< 110.0$ | $< 16.2$ |
| $K^{*+}K^-\pi^+\pi^-$ + c.c. | $-3.0\pm131.2\pm24.5\pm0.3^z$ | $< 218.9$ | $< 32.3$ |
| $\phi\pi^+\pi^-\pi^0$ | $< 25.5^{tn}$ | $< 25.5$ | $< 3.8$ |
| $\Lambda\bar{\Lambda}\pi^0$ | $< 7.9^{tn}$ | $< 7.9$ | $< 1.2$ |

where $N^{\rm up}$ is the upper limit on the number of the signal events for $e^+e^-\to f$, and $\Delta_{\rm sys}$ is the systematic error in the measurement of the observed cross section. Inserting the corresponding numbers in (2), we obtain the upper limits on the observed cross sections for these final states at $\sqrt{s}=3.773$ and 3.650 GeV, respectively, which are shown in Tables 1 and 2.

### 6.4 Upper limits on the observed cross section and the branching fraction for $\psi(3770)\to f$

The upper limits $\sigma^{\rm up}_{\psi(3770)\to f}$ on the observed cross sections for $\psi(3770)$ decay to the final states $\omega\pi^+\pi^-$, $\omega K^+K^-$, $\omega p\bar{p}$, $K^+K^-\rho^0\pi^0$, $\phi\pi^+\pi^-\pi^0$ and $\Lambda\bar{\Lambda}\pi^0$ are directly set based on the upper limits on their observed cross sections at 3.773 GeV.

For the other final states, the observed cross section for $\psi(3770)\to f$ is determined by

$$\sigma_{\psi(3770)\to f}=\sigma^{3.773\ {\rm GeV}}_{e^+e^-\to f}-f_{\rm co}\times\sigma^{3.650\ {\rm GeV}}_{e^+e^-\to f}\,, \qquad (3)$$

where $f_{\rm co}$ is the normalization factor in which we take into account the $1/s$ dependence of the cross section and neglect the difference in the corrections for the ISR and vaccum polarization effects between the two energy points. Inserting the values of $\sigma^{3.773\ {\rm GeV}}_{e^+e^-\to f}$ and $\sigma^{3.650\ {\rm GeV}}_{e^+e^-\to f}$ listed in Tables 1 and 2, and $f_{\rm co}$ in (3), we obtain the $\sigma_{\psi(3770)\to f}$ for each mode, as shown in the second column of Table 3, where the first error is the statistical, the second is the independent systematic error (arising from the uncertainties in the Monte Carlo statistics, in fitting to the mass spectrum and in the background subtraction), and the third is the common systematic error (arising from the other uncertainties as discussed in the Sect. 6.2). The upper limits $\sigma^{\rm up}_{\psi(3770)\to f}$ on the observed cross sections for $\psi(3770)$ decay to these final states are set by shifting the cross sections by $1.64\sigma$, where the $\sigma$ is the total error of the measured cross section. We treat $\sigma_{\psi(3770)\to f}$ with minus value as zero, and then set its upper limit. The third column of Table 3 shows the results on $\sigma^{\rm up}_{\psi(3770)\to f}$.

The upper limit on the branching fraction for $\psi(3770)\to f$ is set by

$$\mathcal{B}^{\rm up}_{\psi(3770)\to f}=\frac{\sigma^{\rm up}_{\psi(3770)\to f}}{\sigma^{\rm obs}_{\psi(3770)}\times\left[1-\Delta\sigma^{\rm obs}_{\psi(3770)}\right]}\,, \qquad (4)$$

where $\sigma^{\rm obs}_{\psi(3770)}$ is the observed cross section for the $\psi(3770)$ production, $\Delta\sigma^{\rm obs}_{\psi(3770)}$ is the relative error in $\sigma^{\rm obs}_{\psi(3770)}$. Here, $\sigma^{\rm obs}_{\psi(3770)}=7.15\pm0.27\pm0.27$ nb [10], is obtained by weighting two measurements [4, 29] from BES Collaboration. Inserting the numbers of $\sigma^{\rm up}_{\psi(3770)\to f}$, $\sigma^{\rm obs}_{\psi(3770)}$ and $\Delta\sigma^{\rm obs}_{\psi(3770)}$ in (4), we obtain $\mathcal{B}^{\rm up}_{\psi(3770)\to f}$ for each mode, as shown in the fourth column of Table 3.

## 7 Summary

In summary, by analyzing the data sets taken at $\sqrt{s}=$ 3.773 and 3.650 GeV with the BES-II detector at the BEPC collider, we have measured the observed cross sections for $\omega\pi^+\pi^-$, $\omega K^+K^-$, $\omega p\bar{p}$, $K^+K^-\rho^0\pi^0$, $K^+K^-\rho^+\pi^-$ + c.c., $K^{*0}K^-\pi^+\pi^0$ + c.c., $K^{*+}K^-\pi^+\pi^-$ + c.c., $\phi\pi^+\pi^-\pi^0$ and $\Lambda\bar{\Lambda}\pi^0$ produced in $e^+e^-$ annihilation at the two energy points. Upper limits with 90% confidence level were derived for the observed cross sections and branching fractions for $\psi(3770)$ decay to these final states. We do not observe significant difference between the observed cross sections for most exclusive light hadron final states at the two energy points. However, this does not mean that $\psi(3770)$

does not decay into these final states, since we neglect the interference effects between the continuum and resonance amplitudes. A better way to extract the branching fractions for $\psi(3770) \to$ *exclusive light hadrons* would be to analyze their energy-dependent observed cross sections at more energy points covering both $\psi(3770)$ and $\psi(3686)$ [30] with the coming BES-III detector at the BEPC-II collider. However, the observed cross sections reported in this paper and those reported in [10, 11, 14, 15] provide constraints which could help to understand both the mechanism of the continuum light hadron production and the discrepancy between the observed cross sections for $D\bar{D}$ and $\psi(3770)$ production.

*Acknowledgements.* The BES collaboration thanks the staff of BEPC for their hard efforts. This work is supported in part by the National Natural Science Foundation of China under contracts Nos. 10491300, 10225524, 10225525, 10425523, the Chinese Academy of Sciences under contract No. KJ 95T-03, the 100 Talents Program of CAS under Contract Nos. U-11, U-24, U-25, the Knowledge Innovation Project of CAS under Contract Nos. U-602, U-34 (IHEP), the National Natural Science Foundation of China under Contract No. 10225522 (Tsinghua University).

## References

1. DELCO Collaboration, W. Bacino, et al., Phys. Rev. Lett. **40**, 671 (1978)
2. G. Rong, D.H. Zhang, J.C. Chen, hep-ex/0506051
3. BES Collaboration, M. Ablikim et al., Phys. Lett. B **641**, 145 (2006)
4. BES Collaboration, M. Ablikim et al., Phys. Rev. Lett. **97**, 121 801 (2006)
5. Particle Data Group, 2007 partial update for edition 2008, http://pdg.lbl.gov
6. BES Collaboration, J.Z. Bai et al., HEP & NP **28**, 325 (2004)
7. BES Collaboration, M. Ablikim et al., Phys. Lett. B **605**, 63 (2005)
8. BES Collaboration, M. Ablikim et al., Phys. Rev. D **70**, 077 101 (2004)
9. BES Collaboration, M. Ablikim et al., Phys. Rev. D **72**, 072 007 (2005)
10. BES Collaboration, M. Ablikim et al., Phys. Lett. B **650**, 111 (2007)
11. BES Collaboration, M. Ablikim et al., arXiv:hep-ex/0710.0786
12. CLEO Collaboration, N.E. Adam et al., Phys. Rev. Lett. **96**, 082 004 (2006)
13. CLEO Collaboration, T.E. Coans et al., Phys. Rev. Lett. **96**, 182 002 (2006)
14. CLEO Collaboration, G.S. Huang et al., Phys. Rev. Lett. **96**, 032 003 (2006)
15. CLEO Collaboration, G.S. Adams et al., Phys. Rev. D **73**, 012 002 (2006)
16. CLEO Collaboration, D. Cronin-Hennessy et al., Phys. Rev. D **74**, 012 005 (2006)
17. CLEO Collaboration, R.A. Briere et al., Phys. Rev. D **74**, 031 106 (2006)
18. BES Collaboration, J.Z. Bai et al., Nucl. Instrum. Methods A **344**, 319 (1994)
19. BES Collaboration, J.Z. Bai et al., Nucl. Instrum. Methods A **458**, 627 (2001)
20. BES Collaboration, M. Ablikim et al., Phys. Lett. B **597**, 39 (2004)
21. BES Collaboration, Phys. Lett. B **603**, 130 (2004)
22. BES Collaboration, Phys. Lett. B **608**, 24 (2005)
23. BES Collaboration, M. Ablikim et al., Nucl. Phys. B **727**, 395 (2005)
24. Particle Data Group, W.-M. Yao, et al., J. Phys. G **33**, 1 (2006)
25. G.J. Felman, R.D. Cousins, Phys. Rev. D **57**, 3873 (1998)
26. BES Collaboration, M. Ablikim et al., Nucl. Instrum. Methods A **552**, 344 (2005)
27. E.A. Kuraev, V.S. Fadin, Yad. Fiz. **41**, 377 (1985)
28. E. Barberio, Z. Was, Comput. Phys. Commun. **79**, 291 (1994)
29. BES Collaboration, M. Ablikim et al., Phys. Lett. B **652**, 238 (2007)
30. BES Collaboration, G. Rong, Int. J. Mod. Phys. A **21**, 5416 (2006)